# One-half magnetization plateau in the spin-$\frac{1}{2}$ fcc lattice antiferromagnet $Sr_2CoTeO_6$

Hidekazu Tanaka,[1,2,*] Akira Matsuo,[3] and Koichi Kindo[3]

[1]*Innovator and Inventor Development Platform, Tokyo Institute of Technology, Midori-ku, Yokohama 226-8502, Japan*
[2]*Department of Physics, Tokyo Institute of Technology, Meguro-ku, Tokyo 152-8551, Japan*
[3]*Institute for Solid State Physics, The University of Tokyo, Kashiwa, Chiba 277-8581, Japan*

(Received 19 December 2023; revised 5 February 2024; accepted 27 February 2024; published 12 March 2024)

We report the results of high-field magnetization measurements on a powdered sample of $Sr_2CoTeO_6$, which approximates the spin-1/2 fcc lattice Heisenberg antiferromagnet. This compound undergoes a magnetic ordering into a type-I antiferromagnetic state at $T_N = 13.4$ K. The magnetization exhibits a plateau at one-half of the saturation magnetization. This indicates antiferromagnetic nearest-neighbor and ferromagnetic next-nearest-neighbor exchange interactions, consistent with the type-I antiferromagnetic state. However, the one-half magnetization plateau is indistinct. This can be ascribed to the small exchange anisotropy or the significant finite-temperature effect due to the energy structure characteristic of the spin-1/2 fcc lattice Heisenberg antiferromagnet. The observed transition sequence is consistent with the theory, although the magnetization anomalies are not sharp.

DOI: 10.1103/PhysRevB.109.094414

## I. INTRODUCTION

Quantum many-body effects have been central topics in condensed matter physics. It is known that spin-1/2 triangular- and kagome-lattice Heisenberg antiferromagnets, prototypical frustrated quantum magnets, produce remarkable quantum many-body effects caused by the synergy between the geometrical frustration and quantum effect [1–3]. Theoretical and experimental studies established that these quantum magnets display the magnetization plateau, a macroscopic quantum many-body effect [4–34]. These frustrated quantum magnets also exhibit fractionalized spin excitations, regardless of whether their zero-field ground states are ordered [35–49]. This strongly suggests that their ground states have a sizable spin-liquid component.

In this context, the study of quantum many-body effects in three-dimensional (3D) frustrated magnets such as spin-1/2 fcc and pyrochlore-lattice Heisenberg antiferromagnets is of interest. The magnetization process in the 3D frustrated magnet has been extensively studied for the spin-3/2 pyrochlore-lattice Heisenberg antiferromagnet, which displays the one-half magnetization plateau caused by the effective biquadratic exchange interaction arising from the spin-lattice coupling [50–52]. Theories showed that the one-half magnetization plateau emerges in spin-1/2 fcc and pyrochlore-lattice Heisenberg antiferromagnets [53–56]. However, its experimental verification is little.

This paper reports on the result of magnetization measurement on a double-perovskite compound $Sr_2CoTeO_6$ using pulsed high magnetic fields. This system can be described as a spin-1/2 Heisenberg-like antiferromagnet on an fcc lattice at low temperatures. Figure 1(a) shows the crystal structure of $Sr_2CoTeO_6$, which is monoclinic $P2_1/n$ with lattice constants of $a = 5.64$ Å, $b = 5.61$ Å, $c = 7.92$ Å, and $\beta = 90.1^\circ$ [57,58]. Taking $\boldsymbol{a}' = \boldsymbol{a} + \boldsymbol{b}$ and $\boldsymbol{b}' = \boldsymbol{b} - \boldsymbol{a}$, we see that magnetic $Co^{2+}$ ions form an fcc lattice, as shown in Fig. 1(b). Although the fcc lattice is distorted, the crystal lattice is close to the uniform fcc lattice because $\sqrt{2}a \approx \sqrt{2}b \approx c$ and $\beta \approx 90^\circ$. $CoO_6$ and $TeO_6$ octahedra are arranged alternately, sharing their corners. Because the nonmagnetic $Te^{6+}$ ion has the filled outermost $4d$ orbital, we can expect that the nearest-neighbor (NN) exchange interaction $J_1$ shown in Fig. 2(a) becomes antiferromagnetic ($J_1 > 0$) and dominant, as discussed in Refs. [59,60].

$Sr_2CoTeO_6$ undergoes a magnetic phase transition at $T_N = 15-18$ K [57,58]. Neutron diffraction experiments determined the magnetic structure in the ordered state to be the type-I antiferromagnetic structure illustrated in Fig. 2(b) [57,58]. The type-I antiferromagnetic structure is realized when the NN interaction $J_1$ is antiferromagnetic, and the next-nearest-neighbor (NNN) interaction $J_2$ is ferromagnetic or very weakly antiferromagnetic ($J_2 \lessapprox 0$) [53,54,61–65]. The type-I antiferromagnetic state was also found in other double-perovskite magnets $Ba_2YRuO_6$ [66] and $Ba_2YOsO_6$ [67], in which magnetic ions are $Ru^{5+}$ and $Os^{5+}$ with spin 3/2. The nonmagnetic hexavalent ion plays an essential role in exchange interactions. $Sr_2CoWO_6$ and $Sr_2NiWO_6$ have a type-II antiferromagnetic structure illustrated in Fig. 2(c) [68,69], which is realized when $J_2$ is antiferromagnetic and $J_2/J_1 \gtrsim 0.5$ [53,54,63–65]. This is because the filled outermost orbital of the $W^{6+}$ ion is $5p$, as discussed in Refs. [59,60].

The magnetic properties of $Co^{2+}$ in an octahedral environment can be described with an effective spin-1/2 when the temperature $T$ is much lower than the magnitude of the spin-orbit coupling constant $\lambda = -178$ cm$^{-1}$, i.e., $T \ll |\lambda|/k_B \simeq 250$ K [70–72]. Hence, the effective spin-1/2 model is valid in the temperature range below the liquid

*tanaka.h.ag@m.titech.ac.jp

 

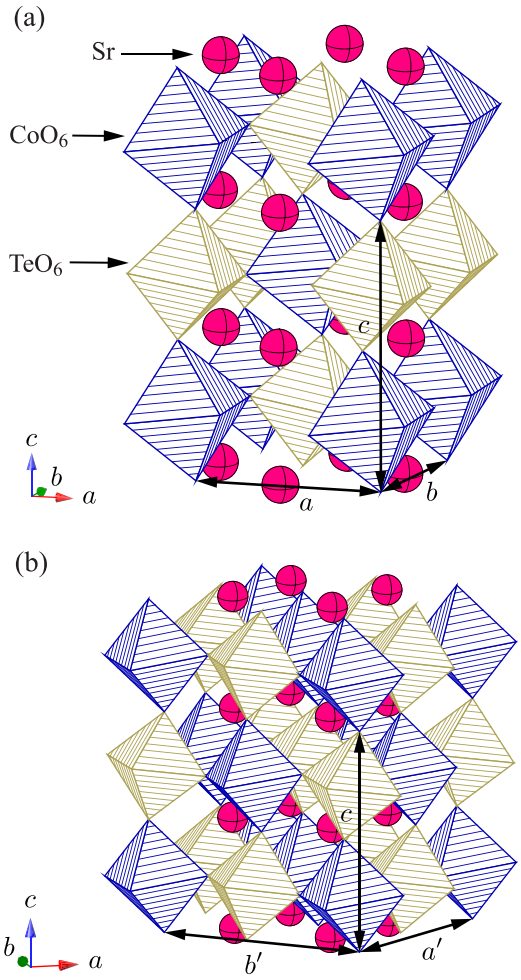


FIG. 1. (a) Schematic view of the crystal structure of $Sr_2CoTeO_6$. The blue and gold octahedra are $CoO_6$ and $TeO_6$ octahedra centered by $Co^{2+}$ and $Te^{6+}$ ions, respectively. (b) Schematic view of an fcc lattice obtained by taking $\boldsymbol{a}' = \boldsymbol{a} + \boldsymbol{b}$ and $\boldsymbol{b}' = \boldsymbol{b} - \boldsymbol{a}$.

nitrogen temperature 77 K. Since the crystal lattice of $Sr_2CoTeO_6$ approximates the cubic fcc lattice, the exchange interaction between the effective spins will be close to the Heisenberg model [71]. The $g$ factor for the Zeeman term will be roughly twice the conventional $g = 2$ [70,71]. The saturation field for the fcc lattice Heisenberg antiferromagnet becomes large even for the spin-1/2 case because the coordination number is 12. It will often exceed the accessible field range. However, using a pulsed high magnetic field up to 73 T, we could observe the entire magnetization process in $Sr_2CoTeO_6$ because of the large $g$ factor, as shown below.

Figure 3(a) shows four sublattices and spin configurations of the type-I antiferromagnetic state stabilized in magnetic fields when $J_1 > 0$ and $J_2 \lessapprox 0$ [53,54,61–65]. The magnetization curve of the spin-1/2 fcc lattice Heisenberg antiferromagnet without the NNN interaction ($J_2 = 0$) was calculated through a cluster mean-field method, assuming a four-sublattice model shown in Fig. 3(a) [55]. Figures 3(b)–3(e) show the spin configurations in magnetic fields. An antiferromagnetic (b) state is stable in zero and low magnetic fields. With increasing magnetic field, quantum fluctuations

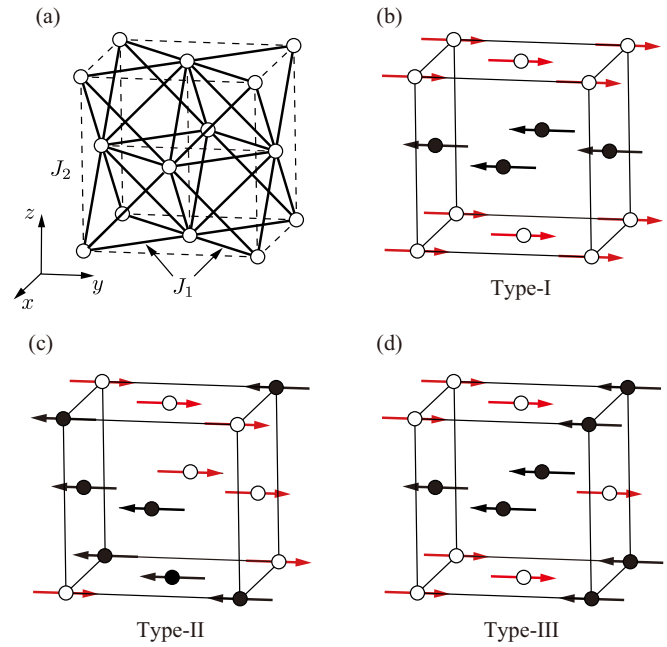


FIG. 2. (a) The exchange network in an fcc lattice antiferromagnet. Thick solid and thin dashed lines denote the nearest-neighbor $J_1$ and the next-nearest-neighbor $J_2$ exchange interactions, respectively. (b) Type-I, (c) type-II, and (d) type-III antiferromagnetic states characterized by propagation vectors $\boldsymbol{q} = (0,\ 0,\ 1)$, $(1/2,\ 1/2,\ 1/2)$, and $(0,\ 1/2,\ 1)$, respectively.

stabilize low-field coplanar (c), up-up-up-down (*uuud*) (d), and high-field coplanar (e) states in this order [53–55]. The magnetization has a plateau at one-half of the saturation magnetization in the *uuud* state. The transition between (b) and (c) states is the first order [55].

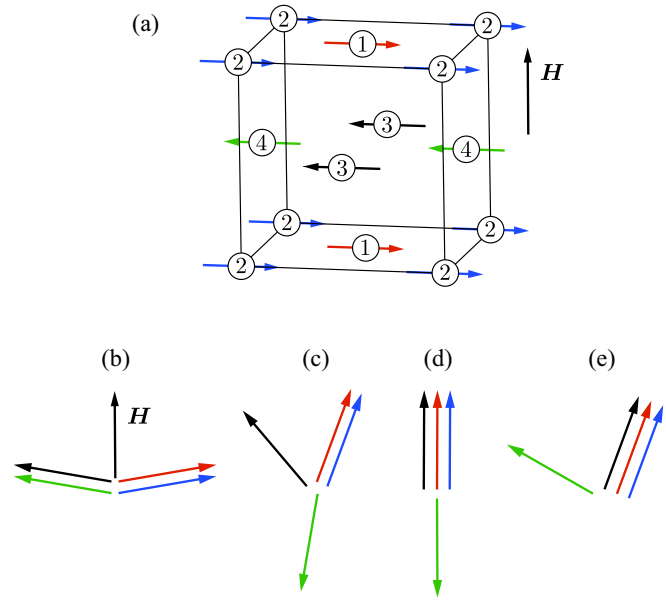


FIG. 3. (a) Four spin sites of the type-I fcc lattice antiferromagnet in magnetic fields. (b)–(e) Possible spin configurations in magnetic fields. (b) Antiferromagnetic, (c) low-field coplanar, (d) collinear up-up-up-down, and (e) high-field coplanar states.

When the $J_1$ and $J_2$ interactions are antiferromagnetic, and $J_2/J_1$ is small, the zero-field ground state is the type-III antiferromagnetic state illustrated in Fig. 2(d) [53,54,61,63–65]. The type-III antiferromagnetic state was observed in $K_2IrCl_6$ [73,74]. With increasing antiferromagnetic $J_2$ from zero, four spin states shown in Figs. 3(b)–3(e) become rapidly unstable [54]. The one-half magnetization plateau is absent in the parameter range for the type-II and -III antiferromagnetic states [54]. The antiferromagnetic $J_2$ interaction strongly suppresses the one-half magnetization plateau.

We observed a one-half magnetization plateau in $Sr_2CoTeO_6$. This observation and the type-I antiferromagnetic state at zero field confirm that $J_1 > 0$ and $J_2 \lessapprox 0$ in $Sr_2CoTeO_6$.

## II. EXPERIMENTAL DETAILS

$Sr_2CoTeO_6$ powder was prepared by the solid-state reaction in accordance with the chemical reaction $2SrO+CoO+TeO_2+\frac{1}{2}O_2 \longrightarrow Sr_2CoTeO_6$. Reagent-grade source materials were mixed in stoichiometric quantities and fired at 900 °C in air for 24 h. The powder was then reground, pelletized, and calcined twice at 1000 °C in air for 24 h. The samples obtained were examined by x-ray powder diffraction.

The magnetic susceptibility of $Sr_2CoTeO_6$ powder was measured in the temperature range of 1.8–300 K using a superconducting quantum interference device (SQUID) magnetometer (MPMS XL, Quantum Design). High-field magnetization was measured in a magnetic field of up to 73 T at 1.3 K using an induction method with a multilayer pulse magnet at the Institute for Solid State Physics, University of Tokyo. The absolute value of the high-field magnetization was calibrated with the magnetization measured using the SQUID magnetometer.

## III. RESULTS AND DISCUSSION

Figure 4(a) shows the temperature dependence of the raw magnetic susceptibility $\chi_r$ and its temperature derivative $d\chi_r/dT$ of $Sr_2CoTeO_6$ powder. The temperature range is below 80 K, where the effective spin-1/2 model holds. The temperature dependence of $\chi_r$ almost coincides with the previous reports [57,58]. A magnetic phase transition is clearly observed at $T_N = 13.4$ K, at which $d\chi_r/dT$ shows a sharp peak. This transition temperature is somewhat lower than $T_N = 15$–$18$ K reported previously [57,58].

We also plotted in Fig. 4(a) the magnetic susceptibility $\chi_c$ after the correction of the Van Vleck paramagnetic susceptibility $\chi_{VV} = 8.27\times10^{-3}$ emu/mol, which was obtained by a high-field magnetization measurement shown below. Figure 4(b) shows the temperature dependences of the magnetic susceptibility $\chi_c$ and its inverse. The solid line is the Curie-Weiss fit with the Curie constant $C = 1.24$ emu K/mol and Weiss temperature $\Theta = -76.9$ K in a $50 \leqslant T \leqslant 80$ K range. We obtain $g_{CW} = 3.63$ from the Curie constant. The $g$ factor is larger than $g_{mag} = 3.08$ obtained from the high-field magnetization measurement below. This is because there is no temperature range below 80 K in which $\chi_c^{-1}$ is precisely linear in $T$ due to the short-range spin correlation.

Figure 5(a) shows the raw magnetization curve and its field derivative $dM/dH$ of $Sr_2CoTeO_6$ powder measured

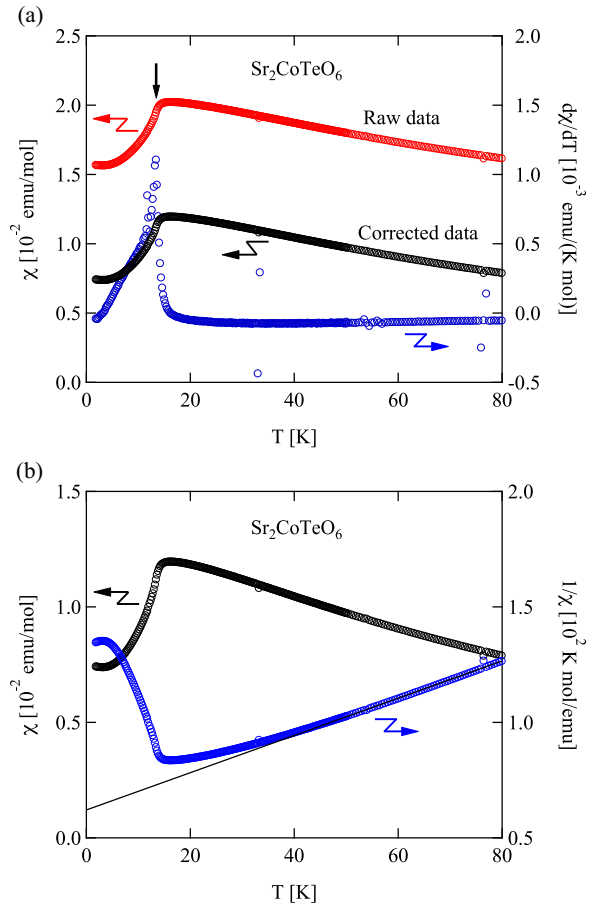


FIG. 4. (a) Temperature dependences of the magnetic susceptibility of $Sr_2CoTeO_6$ powder before and after the correction of the Van Vleck paramagnetism $8.27\times10^{-3}$ emu/mol (left axis), and the temperature derivative of the magnetic susceptibility $d\chi/dT$ (right axis). A vertical arrow denotes the magnetic phase transition temperature $T_N = 13.4$ K. (b) Temperature dependences of the magnetic susceptibility and inverse susceptibility corrected for the Van Vleck paramagnetism. The solid line is the Curie-Weiss fit in a $50 \leqslant T \leqslant 80$ K range.

at $T = 1.3$ K. The magnetization saturates at $H_s = 66.7$ T, at which $dM/dH$ has an inflection point. The magnetization increases after the saturation because of the large Van Vleck paramagnetism characteristic of $Co^{2+}$ in an octahedral environment [71,72]. From the magnetization slope above $H_s$, we evaluated the temperature-independent Van Vleck paramagnetic susceptibility as $\chi_{VV} = 1.48\times10^{-2}\,(\mu_B/T)/Co^{2+} = 8.27\times10^{-3}$ emu/mol. We subtracted $\chi_{VV}$ from the raw magnetic susceptibility $\chi_r$ to obtain the low-temperature spin susceptibility $\chi_c$, as shown in Fig. 4. The saturation magnetization was obtained as $M_s = 1.54\,\mu_B/Co^{2+}$ by extrapolating the magnetization curve above $H_s$ to a zero field [dashed line in Fig. 5(a)]. The $g$ factor is obtained to be $g_{mag} = 3.08$. This $g$ factor is almost the same as $g_{mag} = 3.0$ in $Ba_3CoNb_2O_9$ [59] and smaller than $g_{mag} = 3.82$ in $Ba_3CoSb_2O_9$ [16]. Using a relation $g\mu_B H_s = 8J_1$ and $g_{mag} = 3.08$, we obtain the exchange constant of $J_1/k_B = 17.3$ K.

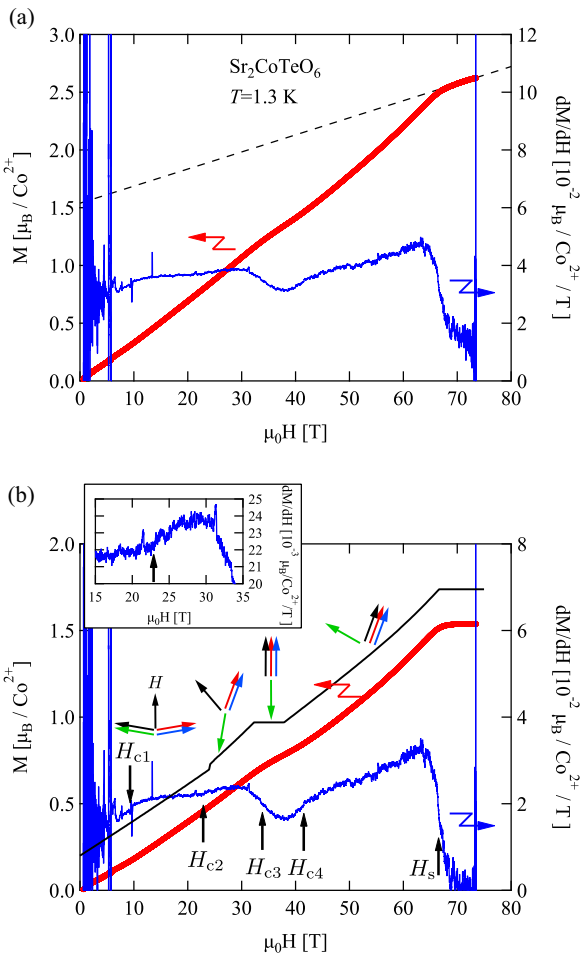


FIG. 5. (a) Raw magnetization curve of $Sr_2CoTeO_6$ powder measured at 1.3 K (left axis) and field derivative susceptibility $dM/dH$ vs magnetic field $H$ (right axis). The dashed line denotes the Van Vleck paramagnetism evaluated from the magnetization slope above the saturation field $H_s = 66.7$ T. (b) Magnetization curve and $dM/dH$ vs $H$ after the correction of the Van Vleck paramagnetism. Vertical arrows are the saturation field and estimated critical fields. The solid black line is the magnetization curve for $J_2 = 0$ calculated by a cluster mean-field method for 28 spin sites [55]. Corresponding spin states are illustrated. The inset shows the expansion of $dM/dH$ between 15 and 35 T.

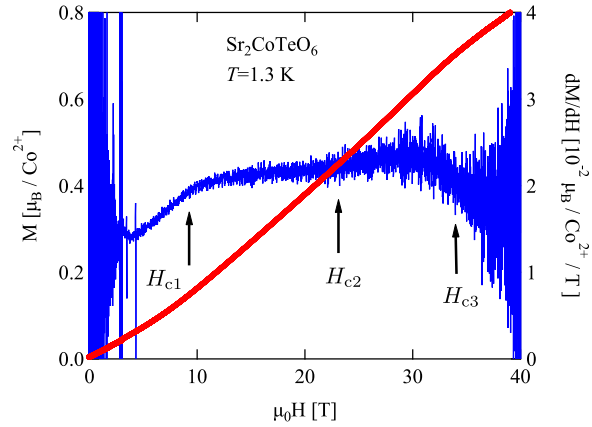


FIG. 6. Magnetization curve of $Sr_2CoTeO_6$ powder after the correction of the Van Vleck paramagnetism measured at 1.3 K using a pulsed magnetic field up to 40 T (left axis) and $dM/dH$ vs $H$ (right axis). Vertical arrows are roughly estimated critical fields.

Figure 5(b) shows the magnetization curve after correcting the Van Vleck paramagnetism. A plateau anomaly is observed at one-half of the saturation magnetization. The lower and higher edge fields are roughly estimated as $H_{c3} \simeq 34$ T and $H_{c4} \simeq 42$ T, shown by vertical arrows. We specified these fields where $dM/dH$ shows inflection points. For comparison, we depicted the magnetization curve for a spin-1/2 fcc lattice Heisenberg antiferromagnet with $J_2 = 0$ calculated by a cluster mean-field method for 28 spin sites [55]. Although the observed one-half plateau is indistinct, it is consistent with the theory of the spin-1/2 fcc lattice Heisenberg antiferromagnet [53–55].

The field derivative of magnetization $dM/dH$ displays a slight bend anomaly at $H_{c2} \simeq 23$ T, as shown in the inset of Figs. 5(b) and 6. This anomaly appears to be the transition between the antiferromagnetic (b) and low-field coplanar (c) states in Fig. 3. The emergence of the one-half magnetization plateau and the type-I antiferromagnetic state observed at zero field confirm that $Sr_2CoTeO_6$ is described as a spin-1/2 fcc lattice Heisenberg-like antiferromagnet with dominant antiferromagnetic $J_1$ and weak ferromagnetic or very weak antiferromagnetic $J_2$ interactions. The $J_2$ interaction is negligible in $Sr_2CuTeO_6$ [75] and $SrLaCuSbO_6$ [76], with similar orbital configurations as those in $Sr_2CoTeO_6$. When the ferromagnetic $J_2$ interaction becomes large, the system approaches the classical model, and the quantum magnetization plateau will be suppressed. For these reasons, we can deduce that the magnitude of the $J_2$ interaction is much smaller than that of the $J_1$ interaction in $Sr_2CoTeO_6$.

Another transition is observed in $dM/dH$ at $H_{c1} \simeq 9$ T, shown by a vertical arrow in Fig. 5(b). This transition is more visible in the magnetization process measured using a pulsed magnetic field up to 40 T, shown in Fig. 6, because decreasing the top field reduces mechanical noise at the start and end. Neutron diffraction experiments indicated that the magnetic moment in the ordered state has both the $c$ axis and $ab$ plane components [57,58]. We deduce that the transition at $H_{c1}$ is the spin reorientation to the antiferromagnetic state shown in Fig. 3(b) that gains the Zeeman energy. For the powder sample, ordered moments are distributed isotropically. Although it should be small, the finite exchange anisotropy $\Delta J$ exists in $Sr_2CoTeO_6$ because the fcc lattice is slightly distorted. Due to the exchange anisotropy, a finite magnetic field of an order of $\sqrt{(\Delta J)J}$ is necessary to orient these ordered moments perpendicular to the applied magnetic field.

When the exchange interaction and the $g$ factor are anisotropic, the saturation field depends on the field direction so that the saturation anomaly for the powdered sample is smeared. However, the saturation anomaly in $Sr_2CoTeO_6$ powder is considerably sharp, as shown in Fig. 5(b). This indicates that the anisotropies of the exchange interactions and the $g$ factor are small.

The observed one-half magnetization plateau is not distinct. Here, we discuss the reason. Theories predict that the exchange randomness can make the magnetization plateau

indistinct in triangular- and kagome-lattice quantum magnets [77–79]. Since the saturation anomaly at $H_s$ is considerably sharp, the exchange randomness will be negligible in $Sr_2CoTeO_6$, as in related compounds $Ba_2CoTeO_6$ [80,81] and $Sr_2CuTeO_6$ [60,75]. Hence, we infer that the smearing of the one-half magnetization plateau is not ascribed to the exchange randomness.

Because the crystal lattice of $Sr_2CoTeO_6$ is not correctly cubic, there is a certain amount of exchange anisotropy. In general, the quantum fluctuation energy is smaller than the classical energy. The quantum magnetization plateau is sensitive to the exchange anisotropy. Whether or not the magnetization plateau emerges and its field range will depend on the field direction. This makes the plateau anomaly indistinct in a powdered sample. The exchange anisotropy will be one of the origins of the indistinct one-half magnetization plateau, even though its magnitude will be significantly smaller than the Heisenberg term.

Since the theoretical one-half magnetization plateau range is $\Delta H \simeq 6.6\,\mathrm{T}$ for $J_1/k_B = 17.3$ K, $J_2 = 0$, and $g = 3.08$, the ratio of the measurement temperature $T = 1.3\,\mathrm{K}$ to the plateau range is $k_B T/(g\mu_B \Delta H) \sim 0.1$. The observed one-half magnetization plateau is indistinct, although the temperature is sufficiently lower than the plateau range. Such a significant finite-temperature effect is also known on the one-third magnetization plateau for the spin-1/2 kagome-lattice Heisenberg antiferromagnet [32,82]. The one-third plateau melts rapidly by the slight temperature increase due to many excited states with different total spins energetically close to the plateau state [82]. This situation will be similar to the case of the one-half magnetization plateau in the spin-1/2 fcc lattice Heisenberg antiferromagnet. The one-half magnetization plateau is destabilized by the antiferromagnetic NNN exchange interaction $J_2$ and disappears very rapidly with increasing the antiferromagnetic $J_2$ [54]. This indicates that many excited states with different total spins are energetically close to the one-half plateau state because the $J_2$ interaction is weak in $Sr_2CoTeO_6$. These excited states give rise to the rapid melting of the one-half plateau with only a tiny temperature increase. Hence, the remarkable finite-temperature effect is also one of the origins of the indistinct one-half magnetization plateau.

## IV. CONCLUSION

We have presented the results of high-field magnetization measurements on a powdered sample of $Sr_2CoTeO_6$ that approximates the spin-1/2 fcc lattice Heisenberg antiferromagnet. We observed a one-half magnetization plateau caused by the quantum fluctuation. Because an antiferromagnetic NNN exchange interaction $J_2$ destabilizes the one-half magnetization plateau, the $J_2$ interaction should be weakly ferromagnetic in $Sr_2CoTeO_6$. This is consistent with the type-I antiferromagnetic state below $T_N = 13.4\,\mathrm{K}$. However, the one-half magnetization plateau is indistinct. This can be attributed to the small exchange anisotropy and the significant finite-temperature effect caused by the energy structure characteristic of the spin-1/2 fcc lattice Heisenberg antiferromagnet. Below the plateau field range, we also observed a small magnetization anomaly suggestive of a quantum phase transition between the antiferromagnetic and low-field coplanar states. Although the magnetization anomalies are not sharp in $Sr_2CoTeO_6$ powder, the observed transition sequence is consistent with the theory overall.

## ACKNOWLEDGMENTS

We thank K. Morita for showing us his theoretical data on the magnetization process and for fruitful discussion, and P. Chanlert, M. Watanabe, and N. Kurita for their technical support. This work was supported by Grants-in-Aid for Scientific Research (A) (No. 17H01142) from the Japan Society for the Promotion of Science.

[1] A. Harrison, J. Phys.: Condens. Matter **16**, S553 (2004).
[2] L. Balents, Nature (London) **464**, 199 (2010).
[3] C. Broholm, R. J. Cava, S. A. Kivelson, D. G. Nocera, M. R. Norman, and T. Senthil, Science **367**, eaay0668 (2020).
[4] H. Nishimori and S. Miyashita, J. Phys. Soc. Jpn. **55**, 4448 (1986).
[5] A. V. Chubokov and D. I. Golosov, J. Phys.: Condens. Matter **3**, 69 (1991).
[6] T. Nikuni and H. Shiba, J. Phys. Soc. Jpn. **62**, 3268 (1993).
[7] A. Honecker, J. Phys.: Condens. Matter **11**, 4697 (1999).
[8] J. Alicea, A. V. Chubukov, and O. A. Starykh, Phys. Rev. Lett. **102**, 137201 (2009).
[9] D. J. J. Farnell, R. Zinke, J. Schulenburg, and J. Richter, J. Phys.: Condens. Matter **21**, 406002 (2009).
[10] T. Sakai and H. Nakano, Phys. Rev. B **83**, 100405(R) (2011).
[11] C. Hotta, S. Nishimoto, and N. Shibata, Phys. Rev. B **87**, 115128 (2013).
[12] D. Yamamoto, G. Marmorini, and I. Danshita, Phys. Rev. Lett. **112**, 127203 (2014).
[13] O. A. Starykh, Rep. Prog. Phys. **78**, 052502 (2015).
[14] D. Sellmann, X. F. Zhang, and S. Eggert, Phys. Rev. B **91**, 081104(R) (2015).
[15] T. Coletta, T. A. Tóth, K. Penc, and F. Mila, Phys. Rev. B **94**, 075136 (2016).
[16] Y. Shirata, H. Tanaka, A. Matsuo, and K. Kindo, Phys. Rev. Lett. **108**, 057205 (2012).
[17] T. Susuki, N. Kurita, T. Tanaka, H. Nojiri, A. Matsuo, K. Kindo, and H. Tanaka, Phys. Rev. Lett. **110**, 267201 (2013).
[18] T. Ono, H. Tanaka, H. Aruga Katori, F. Ishikawa, H. Mitamura, and T. Goto, Phys. Rev. B **67**, 104431 (2003).
[19] T. Ono, H. Tanaka, O. Kolomiyets, H. Mitamura, T. Goto, K. Nakajima, A. Oosawa, Y. Koike, K. Kakurai, J. Klenke, P. Smeibidle, and M. Meißner, J. Phys.: Condens. Matter **16**, S773 (2004).
[20] N. A. Fortune, S. T. Hannahs, Y. Yoshida, T. E. Sherline, T. Ono, H. Tanaka, and Y. Takano, Phys. Rev. Lett. **102**, 257201 (2009).
[21] A. Sera, Y. Kousaka, J. Akimitsu, M. Sera, and K. Inoue, Phys. Rev. B **96**, 014419 (2017).

[22] Y. Kojima, M. Watanabe, N. Kurita, H. Tanaka, A. Matsuo, K. Kindo, and M. Avdeev, Phys. Rev. B **98**, 174406 (2018).

[23] J. Xing, L. D. Sanjeewa, J. Kim, G. R. Stewart, A. Podlesnyak, and A. S. Sefat, Phys. Rev. B **100**, 220407(R) (2019).

[24] K. M. Ranjith, S. Luther, T. Reimann, B. Schmidt, Ph. Schlender, J. Sichelschmidt, H. Yasuoka, A. M. Strydom, Y. Skourski, J. Wosnitza, H. Kühne, Th. Doert, and M. Baenitz, Phys. Rev. B **100**, 224417 (2019).

[25] L. Ding, P. Manuel, S. Bachus, F. Grußler, P. Gegenwart, J. Singleton, R. D. Johnson, H. C. Walker, D. T. Adroja, A. D. Hillier, and A. A. Tsirlin, Phys. Rev. B **100**, 144432 (2019).

[26] D. Yamamoto, T. Sakurai, R. Okuto, S. Okubo, H. Ohta, H. Tanaka, and Y. Uwatoko, Nat. Commun. **12**, 4263 (2021).

[27] K. Hida, J. Phys. Soc. Jpn. **70**, 3673 (2001).

[28] J. Schulenburg, A. Honecker, J. Schnack, J. Richter, and H.-J. Schmidt, Phys. Rev. Lett. **88**, 167207 (2002).

[29] A. Honecker, J. Schulenburg, and J. Richter, J. Phys.: Condens. Matter **16**, S749 (2004).

[30] S. Nishimoto, N. Shibata, and C. Hotta, Nat. Commun. **4**, 2287 (2013).

[31] S. Capponi, O. Derzhko, A. Honecker, A. M. Läuchli, and J. Richter, Phys. Rev. B **88**, 144416 (2013).

[32] J. Schnack, J. Schulenburg, and J. Richter, Phys. Rev. B **98**, 094423 (2018).

[33] X. Plat, T. Momoi, and C. Hotta, Phys. Rev. B **98**, 014415 (2018).

[34] H. Yoshida, J. Phys. Soc. Jpn. **91**, 101003 (2022).

[35] W. Zheng, J. O. Fjærestad, R. R. P. Singh, R. H. McKenzie, and R. Coldea, Phys. Rev. B **74**, 224420 (2006).

[36] A. Mezio, C. N. Sposetti, L. O. Manuel, and A. E. Trumper, Europhys. Lett. **94**, 47001 (2011).

[37] E. A. Ghioldi, A. Mezio, L. O. Manuel, R. R. P. Singh, J. Oitmaa, and A. E. Trumper, Phys. Rev. B **91**, 134423 (2015).

[38] E. A. Ghioldi, M. G. Gonzalez, S. S. Zhang, Y. Kamiya, L. O. Manuel, A. E. Trumper, and C. D. Batista, Phys. Rev. B **98**, 184403 (2018).

[39] F. Ferrari and F. Becca, Phys. Rev. X **9**, 031026 (2019).

[40] C. Zhang and T. Li, Phys. Rev. B **102**, 075108 (2020).

[41] J. Ma, Y. Kamiya, T. Hong, H. B. Cao, G. Ehlers, W. Tian, C. D. Batista, Z. L. Dun, H. D. Zhou, and M. Matsuda, Phys. Rev. Lett. **116**, 087201 (2016).

[42] S. Ito, N. Kurita, H. Tanaka, S. Ohira-Kawamura, K. Nakajima, S. Itoh, K. Kuwahara, and K. Kakurai, Nat. Commun. **8**, 235 (2017).

[43] Y. Kamiya, L. Ge, T. Hong, Y. Qiu, D. L. Quintero-Castro, Z. Lu, H. B. Cao, M. Matsuda, E. S. Choi, C. D. Batista, M. Mourigal, H. D. Zhou, and J. Ma, Nat. Commun. **9**, 2666 (2018).

[44] D. Macdougal, S. Williams, D. Prabhakaran, R. I. Bewley, D. J. Voneshen, and R. Coldea, Phys. Rev. B **102**, 064421 (2020).

[45] M. Punk, D. Chowdhury, and S. Sachdev, Nat. Phys. **10**, 289 (2014).

[46] C. Zhang and T. Li, Phys. Rev. B **102**, 195106 (2020).

[47] F. Ferrari, S. Niu, J. Hasik, Y. Iqbal, D. Poilblanc, and F. Becca, SciPost Phys. **14**, 139 (2023).

[48] T. H. Han, J. S. Helton, S. Chu, D. G. Nocera, J. A. Rodriguez-Rivera, C. Broholm, and Y. S. Lee, Nature (London) **492**, 406 (2012).

[49] M. Saito, R. Takagishi, N. Kurita, M. Watanabe, H. Tanaka, R. Nomura, Y. Fukumoto, K. Ikeuchi, and R. Kajimoto, Phys. Rev. B **105**, 064424 (2022).

[50] K. Penc, N. Shannon, and H. Shiba, Phys. Rev. Lett. **93**, 197203 (2004).

[51] H. Ueda, H. A. Katori, H. Mitamura, T. Goto, and H. Takagi, Phys. Rev. Lett. **94**, 047202 (2005).

[52] A. Miyata, H. Ueda, Y. Ueda, Y. Motome, N. Shannon, K. Penc, and S. Takeyama, J. Phys. Soc. Jpn. **81**, 114701 (2012).

[53] M. T. Heinilä and A. S. Oja, Phys. Rev. B **48**, 7227 (1993).

[54] K. Lefmann and C. Rischel, Eur. Phys. J. B **21**, 313 (2001).

[55] K. Morita and T. Tohyama, Phys. Rev. B **99**, 144417 (2019).

[56] I. Hagymási, R. Schäfer, R. Moessner, and D. J. Luitz, Phys. Rev. B **106**, L060411 (2022).

[57] L. Ortega-San Martin, J. P. Chapman, L. Lezama, J. Saánchez-Marcos, J. Rodríguez-Fernández, M. Isabel Arriortua, and T. Rojo, J. Mater. Chem. **15**, 183 (2005).

[58] M. S. Augsburger, M. C. Viola, J. C. Pedregosa, A. Muñoz, J. A. Alonso, and R. E. Carbonio, J. Mater. Chem. **15**, 993 (2005).

[59] K. Yokota, N. Kurita, and H. Tanaka, Phys. Rev. B **90**, 014403 (2014).

[60] T. Koga, N. Kurita, M. Avdeev, S. Danilkin, T. J. Sato, and H. Tanaka, Phys. Rev. B **93**, 054426 (2016).

[61] D. Mukamel and S. Krinsky, Phys. Rev. B **13**, 5065 (1976).

[62] T. Oguchi, H. Nishimori, and Y. Taguchi, J. Phys. Soc. Jpn. **54**, 4494 (1985).

[63] M. S. Seehra and T. M. Giebultowicz, Phys. Rev. B **38**, 11898 (1988).

[64] T. Yildirim, A. B. Harris, and E. F. Shender, Phys. Rev. B **58**, 3144 (1998).

[65] J. Oitmaa, Phys. Rev. B **108**, 014414 (2023).

[66] T. Aharen, J. E. Greedan, F. Ning, T. Imai, V. Michaelis, S. Kroeker, H. Zhou, C. R. Wiebe, and L. M. D. Cranswick, Phys. Rev. B **80**, 134423 (2009).

[67] E. Kermarrec, C. A. Marjerrison, C. M. Thompson, D. D. Maharaj, K. Levin, S. Kroeker, G. E. Granroth, R. Flacau, Z. Yamani, J. E. Greedan, and B. D. Gaulin, Phys. Rev. B **91**, 075133 (2015).

[68] M. C. Viola, M. J. Martínez-Lope, J. A. Alonso, J. L. Martínez, J. M. De Paoli, S. Pagola, J. C. Pedregosa, M. T. Fernández-Díaz, and R. E. Carbonio, Chem. Mater. **15**, 1655 (2003).

[69] C. Su, X.-T. Zeng, K. Sun, D. Sheptyakov, Z. Chen, X.-L. Sheng, H. Li, and W. Jin, Phys. Rev. B **108**, 054416 (2023).

[70] A. Abragam and M. H. L. Pryce, Proc. R. Soc. London A **206**, 173 (1951).

[71] M. E. Lines, Phys. Rev. **131**, 546 (1963).

[72] T. Oguchi, J. Phys. Soc. Jpn. **20**, 2236 (1965).

[73] V. J. Minkiewicz, G. Shirane, B. C. Frazer, R. G. Wheeler, and P. B. Dorain, J. Phys. Chem. Solids **29**, 881 (1968).

[74] K. Siemensmeyer and M. Meschke, Phys. B: Condens. Matter **297**, 204 (2001).

[75] P. Babkevich, V. M. Katukuri, B. Fåk, S. Rols, T. Fennell, D. Pajić, H. Tanaka, T. Pardini, R. R. P. Singh, A. Mitrushchenkov, O. V. Yazyev, and H. M. Rønnow, Phys. Rev. Lett. **117**, 237203 (2016).

[76] M. Watanabe, N. Kurita, H. Tanaka, W. Ueno, K. Matsui, T. Goto, and M. Hagihala, Phys. Rev. B **105**, 054414 (2022).
[77] K. Watanabe, H. Kawamura, H. Nakano, and T. Sakai, J. Phys. Soc. Jpn. **83**, 034714 (2014).
[78] H. Kawamura, K. Watanabe, and T. Shimokawa, J. Phys. Soc. Jpn. **83**, 103704 (2014).
[79] H. Kawamura and K. Uematsu, J. Phys.: Condens. Matter **31**, 504003 (2019).
[80] P. Chanlert, N. Kurita, H. Tanaka, D. Goto, A. Matsuo, and K. Kindo, Phys. Rev. B **93**, 094420 (2016).
[81] P. Chanlert, N. Kurita, H. Tanaka, M. Kimata, and H. Nojiri, Phys. Rev. B **96**, 064419 (2017).
[82] K. Morita, Phys. Rev. B **108**, 184405 (2023).